

# StrokeFusion: Vector Sketch Generation via Joint Stroke-UDF Encoding and Latent Sequence Diffusion

Jin Zhou  
Shenzhen University

Yi Zhou  
Shenzhen University

Pengfei Xu  
Shenzhen University  
<https://pengfeixu.com/>

Hui Huang  
Shenzhen University

## Abstract

*In the field of sketch generation, raster-format trained models often produce non-stroke artifacts, while vector-format trained models typically lack a holistic understanding of sketches, leading to compromised recognizability. Moreover, existing methods struggle to extract common features from similar elements (e.g., eyes of animals) appearing at varying positions across sketches. To address these challenges, we propose **StrokeFusion**, a two-stage framework for vector sketch generation. It contains a dual-modal sketch feature learning network that maps strokes into a high-quality latent space. This network decomposes sketches into normalized strokes and jointly encodes stroke sequences with Unsigned Distance Function (UDF) maps, representing sketches as sets of stroke feature vectors. Building upon this representation, our framework exploits a stroke-level latent diffusion model that simultaneously adjusts stroke position, scale, and trajectory during generation. This enables high-fidelity stroke generation while supporting stroke interpolation editing. Extensive experiments on the QuickDraw dataset demonstrate that our framework outperforms state-of-the-art techniques, validating its effectiveness in preserving structural integrity and semantic features. Code and models will be made publicly available upon publication.*

## 1. Introduction

Sketch generation, as an essential component of computational creativity, significantly accelerates concept visualization and rapid design iteration in numerous fields, including product design, animation, and interactive prototyping. Although humans effortlessly produce and interpret sketches by intuitively capturing holistic structures and local details, existing computational methods fall short of emulating this capability. These limitations manifest as difficulties in cap-

turing global semantic structures, maintaining stroke-level control, and generating visually coherent sketches, thereby limiting their practicality in professional and creative workflows. Consequently, addressing these challenges through tailored computational paradigms is imperative.

Current sketch representations primarily exist in two formats: *raster sketches* capturing visual appearance and *vector sketches* recording stroke trajectories. Raster sketches often contain pixelation artifacts and non-stroke noise, while vector sketches maintain clean, precise stroke trajectories. Vector formats preserve essential drawing semantics but present parsing difficulties due to stroke order ambiguity and coordinate sparsity. Conversely, rasterization simplifies visual processing yet introduces pixelation artifacts and violates sketch-specific drawing constraints (e.g., monochromatic strokes and clean trajectories). Existing sketch generation approaches exhibit three critical limitations: (1) Pixel-based models generate non-stroke artifacts and violate drawing conventions; (2) Vector-based methods fail to capture global structural semantics; (3) Both paradigms struggle with position-invariant feature learning for recurring elements (e.g., eyes in animal sketches).

The decomposition of sketches into semantically meaningful strokes offers promising solutions. Each stroke inherently carries specific semantic roles (e.g., wings of birds, wheels of vehicles) and spatial attributes (position, scale). However, existing methods either lose stroke-level controllability through rasterization or suffer from sequential ambiguity in vector processing. This necessitates a unified representation that combines the structural awareness of raster formats with the editability of vector data.

We present **StrokeFusion**, a two-stage framework addressing these challenges through dual-modal feature learning and latent space diffusion. The first stage introduces *stroke-UDF joint encoding*, where vector strokes are decomposed into normalized primitives and jointly encoded with Unsigned Distance Function (UDF) maps. While

UDFs enhance information density by diffusing 1D strokes into 2D distance fields, they struggle with representing complex intersections—a gap filled by complementary vector features. This stage produces disentangled stroke embeddings with explicit position/scale parameters.

The second stage introduces a *stroke-level latent diffusion model* that generates strokes in an unordered and non-autoregressive manner. Instead of relying on a fixed generation order, our model learns to predict position, scale, and trajectory jointly by leveraging the stroke embeddings.

Our contributions are threefold:

- A dual-modal encoding framework that synergizes vector strokes with UDF-derived raster features, overcoming individual representation limitations while preserving stroke semantics and spatial attributes
- Disentangled learning of stroke position/scale and shape information, enabling extraction of common patterns from strokes. This decomposes sketch generation into two manageable sub-tasks: stroke layout prediction and shape synthesis, ensuring global structural consistency.
- A diffusion model for sketch generation that encodes each stroke independently, supporting the non-autoregressive generation of unordered, varied-length stroke sequences. This overcomes the limitation of conventional sequential models that require a fixed generation order.

Extensive experiments demonstrate that our method significantly outperforms baseline approaches by leveraging stroke-sketch hierarchical structures. Both quantitative metrics and qualitative comparisons reveal the advantages of our framework. Ablation studies on dual-modal encoding, stroke latent space, and spatial information disentanglement further validate the effectiveness of our design choices.

## 2. Related Work

**Raster Sketch Generation.** Raster sketch generation can be viewed as a stylized image generation problem, where the core challenge lies in producing images with sketch-like styles. Isola et al. [16] proposed conditional Generative Adversarial Networks (cGANs) to translate input images into raster sketches by incorporating “sketch style” as a generation condition. Building on this, Seo et al. [25], Yun et al. [40], and Yang et al. [38] extended GAN applications to enable both sketch-style generation and style feature integration using stylized sketches as constraints. Yun et al. [39] further implemented image-to-raster sketch style transfer via diffusion models, while Hu et al. [14] leveraged guided diffusion models [7] to generate high-quality sketches of simple objects. Most raster sketch generation tasks perform style transfer from general image generation to the sketch domain, resulting in sketches that appear plausible visually but cannot be practically drawn through strokes.

**Parametric Curves.** SVG primitives require diverse parameterizations (e.g., line endpoints, Bézier control points).

Carlier et al. [5] modeled hierarchical relationships between SVG commands, groups, and global features. Wu et al. [33] combined CLIP [23] features with autoregressive models for text-conditioned icon generation. Wang et al. [32] fused rendering instructions and rasterized images for stylized font generation. This representation often introduces ambiguity, making it challenging for models to learn its patterns.

To handle representation ambiguity, some works simplify instructions to uniform primitives (e.g., quadratic Bézier curves). Li et al. [19] introduced differentiable rendering for optimization. Ma et al. [21] proposed hierarchical vectorization via iterative Bézier curve addition. Frans et al. [9] optimized Bézier curves using CLIP for text-to-vector synthesis. Xing et al. [34, 35] generated initial shapes followed by text-guided optimization. Hu et al. [15] integrated differentiable renderers into training. However, open-stroke sketches with sparse rendering regions limit supervision effectiveness. Vinker et al. [29, 30] optimized curve parameters using similarity metrics, while Ashcroft et al. [2] mapped curves to implicit spaces for diffusion-based generation, requiring post-processing to reconnect fragmented strokes. These methods have respective strengths and weaknesses, but currently, the most mainstream and straightforward vector sketch representation remains point sequence-based vectors.

**Vector Sketch Representation.** Ha et al. [11] introduced a stroke-state-annotated polyline sequence representation. Subsequent works by Ribeiro et al. [24], Xu et al. [36], and Lin et al. [20] enhanced Transformer architectures with local-global attention mechanisms and BERT-inspired self-supervision for sketch recognition and completion. While effective for downstream tasks, these methods focus on feature learning rather than direct generation.

**Vector Sketch Generation.** Qi et al. [22] employed graph convolutional networks (GCNs) [17] to partition sketches into spatially dependent blocks. Tiwari et al. [27] discretized sketches into stroke dictionaries for GPT-based generation. Zang et al. [41] modeled sketches via Gaussian mixture latent spaces. Wang et al. [31] framed generation as a denoising diffusion process, while Das et al. [6] adapted DDPM [3] for stroke sequences. Bandyopadhyay et al. [4] mapped sketches to latent spaces using distance fields inspired by Alaniz et al. [1]. Current generation schemes typically adopt purely autoregressive approaches, which struggle to effectively capture the unordered nature between strokes and the ordered nature within individual strokes. While diffusion models enable unordered generation, the varied-length characteristics of each stroke lead to representation ambiguity when explicitly concatenating stroke sequences. Inspired by recent 3D shape generation works [42], our method encodes each stroke as an individual stroke feature vector, treating these vectors as an unordered set of elements during training.

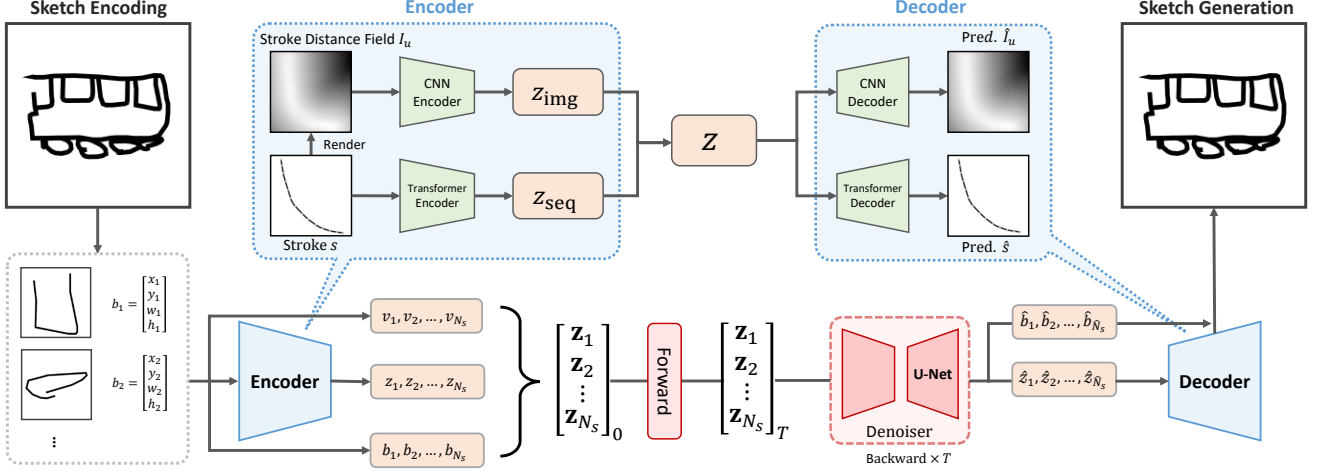


Figure 1. The proposed **StrokeFusion** framework comprises two core components: 1) **Dual-Modal Stroke Encoding**: Each stroke  $s$  is processed through parallel encoding paths - a transformer-based sequence encoder handles geometric coordinates while a CNN processes the stroke distance field  $I_n$ . These modalities are fused into joint features  $f$ , trained via symmetric decoder networks that reconstruct both the original stroke ( $s$ ) and distance field ( $I_n$ ); 2) **Sketch Diffusion Generation**: All normalized strokes are encoded into latent vectors  $z_i$ , augmented with bounding box parameters  $b^i = [x^i, y^i, w^i, h^i]$  and presence flags  $v^i \in \{0, 1\}$ . The diffusion model learns the distribution of stroke sequences  $\{z_1, \dots, z_N\}$  through  $T$ -step denoising training. During generation, the U-Net denoiser progressively refines noisy latents via reverse diffusion, with valid strokes ( $v^i = 1$ ) being decoded through inverse normalization of  $b^i$  to reconstruct the final sketch. The architecture maintains permutation invariance through order-agnostic sequence processing.

**Diffusion Models.** Our work builds on Diffusion Models [26], which operate through forward (gradual noising) and reverse (iterative denoising) processes. Recent advances include continuous-space implementations [7, 13] and discrete-space extensions like D3PM [3]. Gu et al. [10] proposed VQDiffusion with mask-replacement noising, advancing discrete-state diffusion modeling. Our method builds upon these advancements in diffusion modeling while drawing inspiration from recent progress in 3D shape representation [42, 43]. We adapt this vector-set encoding approach to represent artistic strokes, enabling diffusion-based generation of drawing primitives through iterative denoising processes. This combination of discrete-state diffusion techniques with structured vector representations allows our model to benefit from both robust probabilistic modeling and geometrically meaningful feature learning.

### 3. Method

#### 3.1. Problem Formulation and Representation

Existing sketch generation approaches face a fundamental representation dilemma: point-sequence models capture stroke geometry but struggle with visual fidelity, while raster-based methods preserve appearance yet lose structures. This section introduces our dual-modal representation to reconcile these complementary perspectives.

**Vector Representation.** Each stroke  $s_j$  comprises a

point sequence:

$$s_j = \{p_1, p_2, \dots, p_{N_p}\}, \quad p_i = (x_i, y_i, m_i), \quad (1)$$

where  $(x_i, y_i)$  denotes normalized coordinates, and  $m_i \in \{0, 1\}$  indicates pen state. While recurrent networks can model local point relationships, they often fail to preserve visual continuity in rendered strokes due to coordinate-level optimization myopia.

**Visual Representation.** We construct the unsigned distance field  $I_u(g)$  by aggregating stroke density fields [1]. First, define the interpolated point for each consecutive pair:

$$p_i(r) = rx_i + (1 - r)x_{i+1}, \quad r \in [0, 1]. \quad (2)$$

Then compute the segment-wise exponential distance:

$$d_i(g) = \max_{r \in [0, 1]} \exp\left(-\gamma \|g - p_i(r)\|^2\right). \quad (3)$$

Finally, the unsigned distance field is obtained by aggregating these distances:

$$I_u(g) = \max_{i \in \{1, \dots, N_p-1\}} d_i(g), \quad (4)$$

where  $I_u(g)$  is the distance field for stroke  $s_j$ ,  $g$  is the grid point,  $x_i, x_{i+1}$  are consecutive stroke points,  $p_i(r)$  parameterizes linear interpolation between  $x_i$  and  $x_{i+1}$ .

Figure 2 illustrates distance fields of three representative strokes under various decay factors  $\gamma$ .

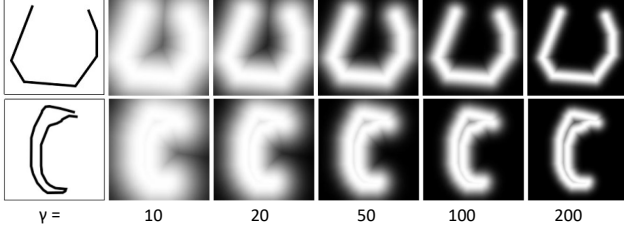


Figure 2. Distance field visualizations of strokes under different decay factors  $\gamma$ . Lower  $\gamma$  values capture overall stroke contours more effectively, whereas higher  $\gamma$  values preserve finer details.

### 3.2. Stroke Embedding

We adopt an encoder-decoder architecture to obtain the neural embeddings of strokes. Our dual-modal encoder jointly processes vector sequences and distance fields through specialized sub-networks, followed by feature fusion, as illustrated in Figure 1.

**Vector Encoder.** Given a stroke point sequence  $s_j = \{p_1, \dots, p_{N_p}\}$ , each point  $p_i = (x_i, y_i, m_i)$  is encoded as:

$$h_i^0 = \text{Linear}(x_i, y_i, m_i) + \text{PE}(i), \quad (5)$$

where  $\text{Linear}(\cdot)$  projects coordinates to  $\mathbb{R}^{d_h}$  and  $\text{PE}(\cdot)$  denotes sinusoidal positional encoding [28]. These initial embeddings  $\{h_i^0\}$  pass through 6 Transformer layers with masked multi-head attention:

$$h_i^{l+1} = \text{TransformerLayer}(h_i^l, \mathbf{M}). \quad (6)$$

The binary mask  $\mathbf{M}$  nullifies invalid positions based on  $m_i$ . Final sequence features  $z_{\text{seq}} \in \mathbb{R}^{d_{\text{seq}}}$  are obtained by mean-pooling the output sequence  $\{h_i^6\}$ .

**Image Encoder.** To extract the visual feature, the unsigned distance field  $I_u$  undergoes 6 convolutional blocks with progressive downsampling:

$$z_{\text{img}}^{(l+1)} = \text{ReLU}(\text{Conv2d}(z_{\text{img}}^{(l)})). \quad (7)$$

Channel dimensions double at each layer from 64 to 512. Global average pooling followed by linear projection yields compact visual features  $z_{\text{img}} \in \mathbb{R}^{d_{\text{img}}}$ .

**Feature Fusion.** The fused stroke representation combines both modalities:

$$z_f = \text{FC}(z_{\text{seq}} \parallel z_{\text{img}}), \quad (8)$$

where  $\parallel$  concatenates along the feature dimension and  $\text{FC}(\cdot)$  projects to  $\mathbb{R}^{d_f}$ . This preserves geometric precision while anchoring visual semantics.

**Stroke Decoders.** Mirroring the encoder structure, the decoder comprises dual pathways for stroke reconstruction. The *vector decoder* employs 6 Transformer layers to regenerate point sequences  $\hat{s} = \{\hat{p}_1, \dots, \hat{p}_{N_p}\}$  from latent features

$\hat{z}_p$ , where each  $\hat{p}_i = (\hat{x}_i, \hat{y}_i, \hat{m}_i)$ . Simultaneously, the *image decoder* utilizes 6 transposed convolutional layers to reconstruct the distance field  $\hat{I}_u$  from  $\hat{z}_u$ . During inference, the image decoder becomes optional, prioritizing sequence-based stroke generation for editability.

### 3.3. Loss Functions

**Vector-level Supervision.** At the vector level, the training is supervised through:

$$\mathcal{L}_{\text{CE}} = \frac{1}{N_p} \sum_{i=1}^{N_p} \text{CE}(m_i, \hat{m}_i), \quad (9)$$

$$\mathcal{L}_1 = \frac{1}{N_p} \sum_{i=1}^{N_p} m_i \|(x_i, y_i) - (\hat{x}_i, \hat{y}_i)\|_1, \quad (10)$$

where CE denotes the cross-entropy loss.  $\mathcal{L}_1$  is computed using a mask derived from  $m_i$ , ensuring coordinates are only penalized when the pen is touching the canvas.

**Image-level Supervision.** At the image level, the UDF image  $I_u$  is compared with the reconstructed image  $\hat{I}_u$  via:

$$\mathcal{L}_{\text{img}} = \|I_u - \hat{I}_u\|_1 + \mathcal{L}_{\text{percep}}(I_u, \hat{I}_u), \quad (11)$$

where  $\mathcal{L}_{\text{percep}}$  is the perceptual loss [44]. Additionally, a KL regularization loss is added to regularize the latent distribution:

$$\mathcal{L}_{\text{KL}} = D_{\text{KL}}(q(z_f|x) \parallel \mathcal{N}(0, I)). \quad (12)$$

The total training loss for the dual-branch stroke encoder is defined as:

$$\mathcal{L}_s = \lambda_{\text{CE}} \mathcal{L}_{\text{CE}} + \lambda_{L_1} \mathcal{L}_1 + \lambda_{\text{img}} \mathcal{L}_{\text{img}} + \lambda_{\text{KL}} \mathcal{L}_{\text{KL}}, \quad (13)$$

where  $\lambda_{\text{CE}}$ ,  $\lambda_{L_1}$ ,  $\lambda_{\text{img}}$ , and  $\lambda_{\text{kl}}$  are the weighting coefficients. This dual-branch design bridges geometric precision (via vector-level supervision) and visual plausibility (via image-level supervision), enabling coordinated learning of stroke topology and appearance.

### 3.4. Diffusion-Based Sketch Generation

The encoder facilitates transformation between individual strokes and their latent representations, while our Sketch Diffusion Generator predicts stroke collections and spatial relationships. This model generates unordered, variable-length stroke sequences as shown in Figure 1.

**Preprocessing.** Our two-stage normalization process ensures geometric consistency:

- **Sketch-level normalization:** center and scale the input sketches to  $[-0.5, 0.5]$  while preserving their aspect ratios. This step standardizes the distribution of stroke bounding boxes.



- **Stroke-level normalization:** independently normalize each stroke’s bounding box coordinates to  $[0.15, 0.85]$  through linear scaling, maintaining individual aspect ratios for geometric relationship preservation.

**Training Process.** During training, each normalized stroke is encoded into a latent embedding  $z_i$  through the dual-modal encoder. A embedding is augmented with its corresponding bounding box parameters  $b_i$  and presence flag  $v_i \in \{0, 1\}$ , forming a composite latent vector:

$$\mathbf{z}_i = [z_i, b_i, v_i].$$

A sequence of such vectors  $\{\mathbf{z}_1, \dots, \mathbf{z}_{N_s}\}$  constitutes the input to the diffusion model. The model learns to progressively denoise latent vectors through a Markov chain of  $T$  diffusion steps, capturing the joint distribution of strokes and their geometric relationships.

**Generation Process.** At inference time, the diffusion model generates a noisy latent sequence  $\{\mathbf{z}_1, \dots, \mathbf{z}_{N_s}\}_T$  that is iteratively refined to  $\{\mathbf{z}_1, \dots, \mathbf{z}_{N_s}\}_0$  via reverse diffusion. Each refined vector  $\{\mathbf{z}_i\}_0$  is decomposed through:

$$[\hat{z}_i, \hat{b}_i, \hat{v}_i] = \text{MLP}_{\text{split}}(\mathbf{z}_i),$$

where  $\hat{v}_i$  indicates stroke validity. Only strokes with  $\hat{v}_i = 1$  are retained and inversely normalized using  $\hat{b}_i$  to recover the original scale and position. The final sketch is rendered by superimposing all valid strokes while maintaining their spatial coherence.

This framework is inherently permutation-invariant due to its order-agnostic processing and enables flexible stroke generation through learned validity flags.

### 3.5. Training Strategy

Training is performed in two sequential stages. First, the encoder-decoder structure is pre-trained using the stroke reconstruction loss  $\mathcal{L}_s$  (including the KL divergence term). Then, in the diffusion stage, the encoder and decoder parameters remain fixed, and a diffusion model is trained to generate coherent latent stroke sets. This two-stage strategy stabilizes training and enhances the structural editability of the generated sketches.

## 4. Experiments

### 4.1. Experimental Setup

**Dataset and Preprocessing.** Our dual-branch stroke encoder and sketch generation diffusion model are trained on the QuickDraw dataset [11]. To evaluate model performance across varying sketch complexities, we select 14 representative categories: *airplane, apple, bus, cat, chair, face, fish, moon, pizza, shoe, spider, television, train, and umbrella*. Following existing works [37], we employ the Ramer-Douglas-Peucker (RDP) algorithm [8] to simplify sketch strokes while preserving their geometric semantics.

**Baseline Methods.** We compare our approach against three baselines: SketchRNN [37], a recurrent neural network supporting temperature-controlled conditional and unconditional generation; SketchKnitter [31]; and ChiroDiff [6]. These baselines represent state-of-the-art methods in stroke-based and diffusion-driven sketch generation.

**Evaluation Metrics.** We adopt three metrics to assess generation quality: Fréchet Inception Distance (FID) [12] for distribution similarity, and Precision/Recall [18] to measure diversity and fidelity. These metrics collectively evaluate how well generated sketches align with real data distributions in both structural coherence and stylistic variability.

### 4.2. Implementation Details

**Stroke Encoder.** The dual-branch stroke encoder employs 6 Transformer layers with a hidden dimension  $d_h = 64$  and processes input sequences truncated to a maximum stroke length  $N_p = 48$ . The unsigned distance field images  $I_u$  are generated at a resolution of  $64 \times 64$ , with feature dimensions  $d_{\text{seq}} = 32$  and  $d_{\text{img}} = 64$ . The model is optimized using Adam with a base learning rate of 0.001, combined with a linear warmup-and-decay schedule over 50 epochs (5 warmup epochs). Training uses a batch size of 256, dropout rate 0.1, and loss weights  $\lambda_{\text{CE}} = 0.1$ ,  $\lambda_{\text{img}} = 0.1$ ,  $\lambda_{L_1} = 1.0$ , and  $\lambda_{\text{KL}} = 0.01$ .

**Diffusion Model.** The sketch generation diffusion model operates over  $T = 1000$  denoising steps, handling sketches with up to  $N_s = 32$  strokes. It utilizes MLP layers with a projection dimension of 512, optimized by AdamW with a base learning rate of 0.0002. Training spans 20 epochs (5 warmup epochs) with a batch size of 128, sharing the same learning rate scheduler as the stroke encoder.

**Training Detail.** For the dual-branch stroke encoder, we adapt training strategies to category-specific complexity. To balance stroke diversity and computational efficiency, we maintain 140,000 to 200,000 training strokes per category by either using all strokes or randomly sampling 50% of strokes from each sketch. All stroke coordinates are normalized to the range  $[0, 1]$  and centrally aligned through isotropic scaling to ensure scale and position invariance. This preprocessing promotes consistent morphological representations and stabilizes feature learning.

The diffusion model for sketch generation is trained on 70,000 complete sketches per category, capturing comprehensive drawing characteristics and variations. This full training set enables the model to learn diverse styles and fine-grained details essential for high-quality generation. Representative samples from the 14 categories are visualized in the supplemental materials.

### 4.3. Quantitative Comparison

**Stroke-Count-Based Analysis.** To systematically evaluate performance across varying sketch complexities, we cate-

Method	< 4 strokes			< 8 strokes			$\geq 8$ strokes		
	FID↓	Prec↑	Rec↑	FID↓	Prec↑	Rec↑	FID↓	Prec↑	Rec↑
SketchRNN	31.607	0.490	0.449	36.978	0.580	0.439	40.667	0.552	0.396
SketchKnitter	23.166	0.518	<u>0.479</u>	27.067	0.571	0.450	35.635	0.541	0.401
ChiroDiff	<b>17.166</b>	0.607	<b>0.496</b>	23.838	0.630	0.452	27.784	0.618	0.418
Ours ( $\gamma = 50$ )	<u>19.532</u>	<b>0.675</b>	0.454	<b>18.901</b>	<b>0.665</b>	<b>0.533</b>	<b>19.173</b>	<b>0.667</b>	<u>0.468</u>
Ours ( $\gamma = 100$ )	20.419	<u>0.662</u>	0.456	<u>18.907</u>	<u>0.664</u>	<u>0.523</u>	<u>19.288</u>	<u>0.659</u>	<b>0.487</b>

Table 1. Performance comparison across different stroke-count categories. Classes are grouped by average stroke counts: low-stroke ( $< 4$ ), medium-stroke ( $< 8$ ), and high-stroke ( $\geq 8$ ). Bold and underlined values indicate the best and second-best performances, respectively.

gorize test classes into three groups by average stroke count: *low-stroke* ( $< 4$  strokes, including apple, moon, shoe, umbrella, and fish), *medium-stroke* ( $< 8$  strokes, including chair, airplane, television, face, and bus), and *high-stroke* ( $\geq 8$  strokes, including pizza, spider, cat, and train). Table 1 compares our method with the baselines using FID, Precision (Prec), and Recall (Rec), where bold and underlined values denote top-two performances.

Our method maintains robust generation quality as stroke complexity increases: it achieves superior FID and Precision-Recall balance for medium- and high-stroke categories. For low-stroke sketches, while our approach attains the highest Precision (0.675 at  $\gamma = 50$ ), FID performance slightly degrades due to insufficient distribution of details across fewer strokes: high-level visual information is less effectively dispersed among limited strokes. Nevertheless, our method remains competitive across all metrics.

#### 4.4. Qualitative Analysis

**Visual Quality.** Figure 3 demonstrates that our method generates sketches with more coherent stroke layouts and richer local details than the baselines. By explicitly modeling the stroke-sketch hierarchy, our approach separates layout planning from detail refinement, yielding structurally natural and visually precise results. This advantage becomes pronounced in complex scenes requiring multi-stroke interactions.

**Denoising Process Visualization.** Figure 4 illustrates the progressive refinement during diffusion sampling. Initial noisy strokes (early steps) gradually evolve into organized patterns, with semantically irrelevant strokes being pruned. Crucially, even at intermediate denoising stages, individual strokes retain well-defined structures and local details. This behavior stems from our dual-branch stroke encoder, which enforces consistent feature learning across the stroke population, enabling high-quality latent space navigation during generation.

#### 4.5. Latent Space Analysis of Stroke Encoding

**Stroke Reconstruction.** We evaluate the dual-branch stroke encoder trained with a distance field decay coefficient

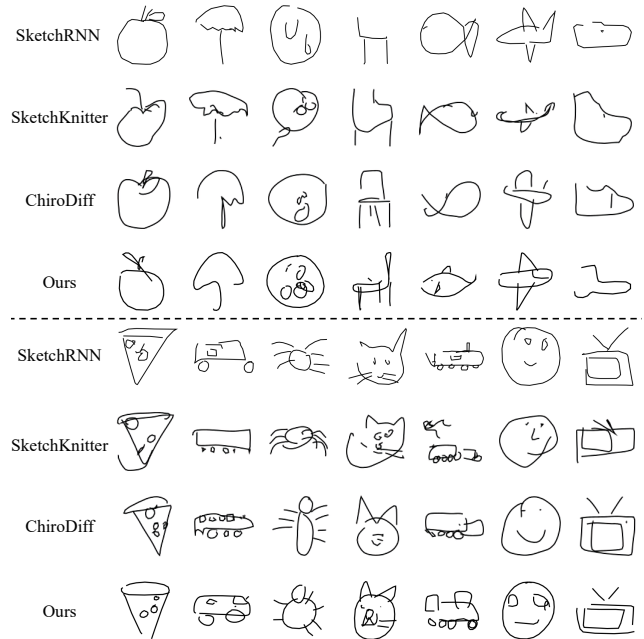


Figure 3. Qualitative comparison of sketches generated by our method and the baselines across different stroke complexities. Our method consistently produces more structurally coherent sketches with richer local details, particularly in complex, multi-stroke scenarios.

$\gamma = 50.0$  through qualitative reconstruction. As shown in Figure 5, the encoder accurately reconstructs strokes across varying complexities, from simple smooth structures to those with intricate local details. This demonstrates its ability to preserve both geometric and visual information in the latent space while capturing essential stroke features.

**Feature Interpolation.** Figure 6 visualizes linear interpolations between stroke features. The intermediate strokes exhibit smooth and semantically meaningful transitions, indicating a well-structured latent space where local geometry variations are continuously encoded. This coherence suggests that the encoder learns disentangled representations of stroke morphology.

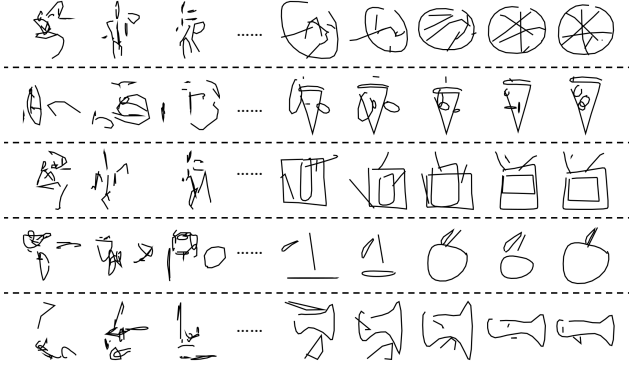


Figure 4. Visualization of diffusion denoising progress. Noise decreases from left to right in each row, demonstrating progressive refinement and pruning of irrelevant strokes.

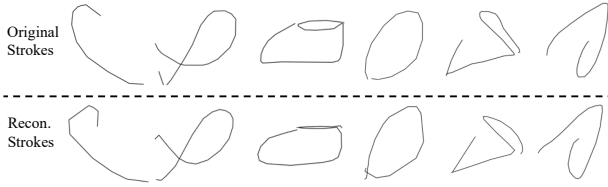


Figure 5. Qualitative comparisons between original and reconstructed strokes.

**Random Sampling.** Figure 7 displays strokes generated by sampling from the latent space. Most samples exhibit clear geometric structures, with some implicitly approximating sketch object contours. While occasional distortions occur, these align with natural sketch-drawing variations, confirming that the latent space encodes plausible stroke distributions. The results validate that the encoder effectively captures fundamental stroke characteristics while allowing controlled diversity.

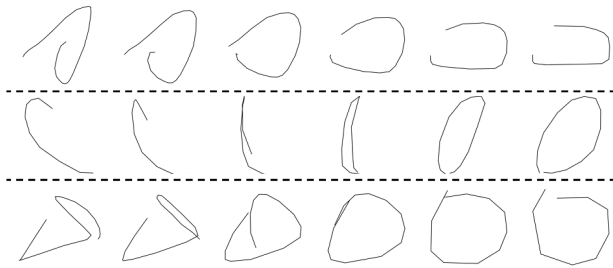


Figure 6. Visualization of stroke interpolation. Each row illustrates a smooth transition of strokes from left to right.



Figure 7. Examples of strokes randomly sampled from the latent space, demonstrating geometric clarity and plausible variations.

## 5. Ablation Study

### 5.1. Stroke Normalization

Our stroke preprocessing involves scaling all strokes to a uniform size and normalizing their positions to be within the range  $[0.15, 0.85]$  in the image coordinates. This ensures that similar strokes, such as circles, have consistent representations from the model’s perspective. Consequently, similar strokes exhibit identical representations, enabling the model to focus solely on intrinsic stroke features rather than global layout variations. This normalization facilitates the encoder to learn stroke characteristics without being distracted by global positioning information.

To evaluate the effectiveness of this normalization, we conducted comparative experiments. Specifically, we trained another stroke encoder without normalizing input strokes, thus directly accepting raw input strokes. Furthermore, this alternative encoder omitted explicit stroke bounding box information, requiring such spatial information to be implicitly encoded in the representation. We selected representative sketch categories spanning low-stroke (moon), medium-stroke (television), and high-stroke complexity (spider) to ensure comprehensive evaluation.

Figure 8 qualitatively demonstrates that omitting normalization results in a noticeable degradation of generation quality. Large structures remain recognizable despite slight distortions, but finer details such as spider legs, television antennas, and lunar craters become severely distorted, often exceeding expected spatial boundaries. In the low-stroke category (moon), stroke structures corresponding to lunar craters are disorganized. For high-stroke sketches (spider), although the basic spider form remains recognizable, detailed structures of legs exhibit significant deviations in position and orientation, resulting in overall visual disorder. This degradation likely stems from increased difficulty in learning consistent patterns from unnormalized data.

Table 2 shows the quantitative results. It demonstrates that the non-normalized method leads to substantial declines in FID, Precision, and Recall metrics, confirming the qualitative observations.

### 5.2. Impact of Image-level Supervision

To examine the influence of the image-level visual branch, we set the decay coefficient  $\gamma = 0$ , effectively removing

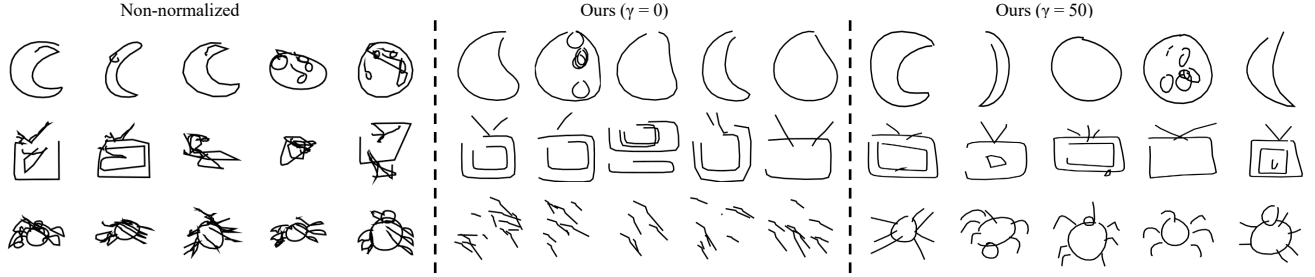


Figure 8. Visualization results of the ablation study. From top to bottom, the rows correspond to the settings without stroke normalization, without distance field image supervision ( $\gamma = 0$ ), and our full model. We select three representative categories with varying stroke complexities: Moon (low-stroke), Television (medium-stroke), and Spider (high-stroke).

Method	moon			television			spider		
	FID↓	Prec↑	Rec↑	FID↓	Prec↑	Rec↑	FID↓	Prec↑	Rec↑
Non-normalized	46.733	0.669	0.035	105.648	0.242	0.030	84.443	0.614	0.021
Ours ( $\gamma = 0$ )	38.027	0.568	0.268	46.519	0.532	0.134	139.279	0.112	0.001
Ours ( $\gamma = 50$ )	<b>24.998</b>	<b>0.678</b>	<b>0.414</b>	<b>16.276</b>	<b>0.630</b>	<b>0.549</b>	<b>15.185</b>	<b>0.708</b>	<b>0.480</b>

Table 2. Quantitative comparisons of stroke normalization and visual supervision. The *Non-normalized* method omits stroke normalization, resulting in degraded sketch fidelity due to inconsistent stroke representations. Setting  $\gamma = 0$  removes image-level visual supervision, substantially compromising generation quality and stroke diversity. Bold values indicate the best performance.

visual information from input distance fields and leaving the image branch to process entirely blank inputs.

**Qualitative Analysis.** Figure 8 illustrates representative outcomes. For low-stroke sketches (moon), stroke directions and structural details, such as craters, become homogeneous and lack diversity. For television sketches, strokes share similar orientations and openings, indicating a loss of richness in stroke hierarchy. Visual recognizability is severely compromised in high-stroke sketches (spider); the generated output consists of scattered, short strokes that fail to form coherent spider shapes. This result likely arises due to the absence of visual supervision, causing the encoder to lose essential stroke differentiation cues.

**Quantitative Analysis.** Table 2 quantitatively compares the sketch generation quality with and without visual supervision. Metrics across categories confirm the qualitative observations: FID and Recall scores substantially decline without image-level guidance, alongside Precision degradation. Overall, these experiments confirm that the proposed stroke encoder fails to effectively capture diverse stroke characteristics without image-level supervision, demonstrating the critical role of visual-level guidance in maintaining sketch fidelity.

### 5.3. Limitations

While our method demonstrates strong performance, some limitations persist. First, complex strokes with high-frequency details remain challenging due to their inherent

data intensity as point sequences. Despite RDP simplification, such strokes occupy disproportionate representation capacity, leading to suboptimal learning efficiency and generation quality for low-stroke sketches. Second, the unsigned distance field (UDF) decoding process introduces computational overhead, as we ultimately rely on point sequences for stroke representation. Future work should explore efficient implicit field decoding schemes or alternative UDF representations to streamline this component. Additionally, since our method generates sketches with strokes as the minimal unit, it requires that the strokes in the dataset contain semantic information. Vector sketches generated by algorithms often feature strokes that span multiple semantic parts, such as an eye and hair being part of the same stroke. This structure prevents our model from producing high-quality results. A potential improvement would be to segment input sketches in a more flexible, symbolically semantic manner, allowing better adaptation to such cases.

## 6. Conclusion

We have presented **StrokeFusion**, a novel framework for vector sketch generation through dual-modal stroke encoding and continuous diffusion modeling. Our dual-branch stroke encoder jointly learns geometric and visual features from both point sequences and distance field images, fusing them into a unified high-quality latent space. This enriched representation enables subsequent continuous diffusion processes to model stroke evolution with smooth feature tran-



sitions, producing sketches with natural fluidity, structural coherence, and enhanced detail quality. Unlike discrete diffusion counterparts, our approach preserves spatial relationships during denoising while maintaining computational efficiency. Comprehensive qualitative and quantitative experiments validate the method’s superiority in generating diverse and structurally plausible sketches across varying complexity levels.

## References

- [1] Stephan Alaniz, Massimiliano Mancini, Anjan Dutta, Diego Marcos, and Zeynep Akata. Abstracting sketches through simple primitives. In *European Conference on Computer Vision*, pages 396–412. Springer, 2022. 2, 3
- [2] Alexander Ashcroft, Ayan Das, Yulia Gryaditskaya, Zhiyu Qu, and Yi-Zhe Song. Modelling complex vector drawings with stroke-clouds. In *The Twelfth International Conference on Learning Representations*, 2023. 2
- [3] Jacob Austin, Daniel D Johnson, Jonathan Ho, Daniel Tarlow, and Rianne Van Den Berg. Structured denoising diffusion models in discrete state-spaces. *Advances in neural information processing systems*, 34:17981–17993, 2021. 2, 3
- [4] Hmrishav Bandyopadhyay, Ayan Kumar Bhunia, Pinaki Nath Chowdhury, Aneeshan Sain, Tao Xiang, Timothy Hospedales, and Yi-Zhe Song. Sketchinr: A first look into sketches as implicit neural representations. In *Proceedings of the IEEE/CVF Conference on Computer Vision and Pattern Recognition*, pages 12565–12574, 2024. 2
- [5] Alexandre Carlier, Martin Danelljan, Alexandre Alahi, and Radu Timofte. Deepsvg: A hierarchical generative network for vector graphics animation. *Advances in Neural Information Processing Systems*, 33:16351–16361, 2020. 2
- [6] Ayan Das, Yongxin Yang, Timothy Hospedales, Tao Xiang, and Yi-Zhe Song. Chirodiff: Modelling chirographic data with diffusion models. *arXiv preprint arXiv:2304.03785*, 2023. 2, 5
- [7] Prafulla Dhariwal and Alexander Nichol. Diffusion models beat gans on image synthesis. *Advances in neural information processing systems*, 34:8780–8794, 2021. 2, 3
- [8] David H Douglas and Thomas K Peucker. Algorithms for the reduction of the number of points required to represent a digitized line or its caricature. *Cartographica: the international journal for geographic information and geovisualization*, 10 (2):112–122, 1973. 5
- [9] Kevin Frans, Lisa Soros, and Olaf Witkowski. Clipdraw: Exploring text-to-drawing synthesis through language-image encoders. *Advances in Neural Information Processing Systems*, 35:5207–5218, 2022. 2
- [10] Shuyang Gu, Dong Chen, Jianmin Bao, Fang Wen, Bo Zhang, Dongdong Chen, Lu Yuan, and Baining Guo. Vector quantized diffusion model for text-to-image synthesis. In *Proceedings of the IEEE/CVF conference on computer vision and pattern recognition*, pages 10696–10706, 2022. 3
- [11] David Ha and Douglas Eck. A neural representation of sketch drawings. *arXiv preprint arXiv:1704.03477*, 2017. 2, 5
- [12] Martin Heusel, Hubert Ramsauer, Thomas Unterthiner, Bernhard Nessler, and Sepp Hochreiter. Gans trained by a two time-scale update rule converge to a local nash equilibrium. *Advances in neural information processing systems*, 30, 2017. 5
- [13] Jonathan Ho, Ajay Jain, and Pieter Abbeel. Denoising diffusion probabilistic models. *Advances in neural information processing systems*, 33:6840–6851, 2020. 3
- [14] Jijin Hu, Ke Li, Yonggang Qi, and Yi-Zhe Song. Scale-adaptive diffusion model for complex sketch synthesis. In *The Twelfth International Conference on Learning Representations*, 2024. 2
- [15] Teng Hu, Ran Yi, Baihong Qian, Jiangning Zhang, Paul L Rosin, and Yu-Kun Lai. Supersvg: Superpixel-based scalable vector graphics synthesis. In *Proceedings of the IEEE/CVF Conference on Computer Vision and Pattern Recognition*, pages 24892–24901, 2024. 2
- [16] Phillip Isola, Jun-Yan Zhu, Tinghui Zhou, and Alexei A Efros. Image-to-image translation with conditional adversarial networks. In *Proceedings of the IEEE conference on computer vision and pattern recognition*, pages 1125–1134, 2017. 2
- [17] Thomas N Kipf and Max Welling. Semi-supervised classification with graph convolutional networks. *arXiv preprint arXiv:1609.02907*, 2016. 2
- [18] Tuomas Kynkäänniemi, Tero Karras, Samuli Laine, Jaakko Lehtinen, and Timo Aila. Improved precision and recall metric for assessing generative models. *Advances in neural information processing systems*, 32, 2019. 5
- [19] Tzu-Mao Li, Michal Lukáč, Michaël Gharbi, and Jonathan Ragan-Kelley. Differentiable vector graphics rasterization for editing and learning. *ACM Transactions on Graphics (TOG)*, 39(6):1–15, 2020. 2
- [20] Hangyu Lin, Yanwei Fu, Xiangyang Xue, and Yu-Gang Jiang. Sketch-bert: Learning sketch bidirectional encoder representation from transformers by self-supervised learning of sketch gestalt. In *Proceedings of the IEEE/CVF Conference on Computer Vision and Pattern Recognition*, pages 6758–6767, 2020. 2
- [21] Xu Ma, Yuqian Zhou, Xingqian Xu, Bin Sun, Valerii Filev, Nikita Orlov, Yun Fu, and Humphrey Shi. Towards layer-wise image vectorization. In *Proceedings of the IEEE/CVF Conference on Computer Vision and Pattern Recognition*, pages 16314–16323, 2022. 2
- [22] Yonggang Qi, Guoyao Su, Qiang Wang, Jie Yang, Kaiyue Pang, and Yi-Zhe Song. Generative sketch healing. *International Journal of Computer Vision*, 130(8):2006–2021, 2022. 2
- [23] Alec Radford, Jong Wook Kim, Chris Hallacy, Aditya Ramesh, Gabriel Goh, Sandhini Agarwal, Girish Sastry, Amanda Askell, Pamela Mishkin, Jack Clark, et al. Learning transferable visual models from natural language supervision. In *International conference on machine learning*, pages 8748–8763. Pmlr, 2021. 2

- [24] Leo Sampaio Ferraz Ribeiro, Tu Bui, John Collomosse, and Moacir Ponti. Sketchformer: Transformer-based representation for sketched structure. In *Proceedings of the IEEE/CVF conference on computer vision and pattern recognition*, pages 14153–14162, 2020. 2
- [25] Chang Wook Seo, Amirsaman Ashtari, and Junyong Noh. Semi-supervised reference-based sketch extraction using a contrastive learning framework. *ACM Transactions on Graphics (TOG)*, 42(4):1–12, 2023. 2
- [26] Jascha Sohl-Dickstein, Eric Weiss, Niru Maheswaranathan, and Surya Ganguli. Deep unsupervised learning using nonequilibrium thermodynamics. In *International conference on machine learning*, pages 2256–2265. pmlr, 2015. 3
- [27] Adarsh Tiwari, Sanket Biswas, and Josep Lladós. Sketchgpt: Autoregressive modeling for sketch generation and recognition. In *International Conference on Document Analysis and Recognition*, pages 421–438. Springer, 2024. 2
- [28] Ashish Vaswani, Noam Shazeer, Niki Parmar, Jakob Uszkoreit, Llion Jones, Aidan N Gomez, Łukasz Kaiser, and Illia Polosukhin. Attention is all you need. *Advances in neural information processing systems*, 30, 2017. 4
- [29] Yael Vinker, Ehsan Pajouheshgar, Jessica Y Bo, Roman Christian Bachmann, Amit Haim Bermano, Daniel Cohen-Or, Amir Zamir, and Ariel Shamir. Clipasso: Semantically-aware object sketching. *ACM Transactions on Graphics (TOG)*, 41(4):1–11, 2022. 2
- [30] Yael Vinker, Yuval Alaluf, Daniel Cohen-Or, and Ariel Shamir. Clipascene: Scene sketching with different types and levels of abstraction. In *Proceedings of the IEEE/CVF International Conference on Computer Vision*, pages 4146–4156, 2023. 2
- [31] Qiang Wang, Haoge Deng, Yonggang Qi, Da Li, and Yi-Zhe Song. Sketchknitter: Vectorized sketch generation with diffusion models. In *The Eleventh International Conference on Learning Representations*, 2023. 2, 5
- [32] Yuqing Wang, Yizhi Wang, Longhui Yu, Yuesheng Zhu, and Zhouhui Lian. Deepvecfont-v2: Exploiting transformers to synthesize vector fonts with higher quality. In *Proceedings of the IEEE/CVF conference on computer vision and pattern recognition*, pages 18320–18328, 2023. 2
- [33] Ronghuan Wu, Wanchao Su, Kede Ma, and Jing Liao. Iconshop: Text-guided vector icon synthesis with autoregressive transformers. *ACM Transactions on Graphics (TOG)*, 42(6):1–14, 2023. 2
- [34] Ximing Xing, Chuang Wang, Haitao Zhou, Jing Zhang, Qian Yu, and Dong Xu. Diffsketcher: Text guided vector sketch synthesis through latent diffusion models. *Advances in Neural Information Processing Systems*, 36:15869–15889, 2023. 2
- [35] Ximing Xing, Haitao Zhou, Chuang Wang, Jing Zhang, Dong Xu, and Qian Yu. Svgdreamer: Text guided svg generation with diffusion model. In *Proceedings of the IEEE/CVF Conference on Computer Vision and Pattern Recognition*, pages 4546–4555, 2024. 2
- [36] Pengfei Xu, Banhuai Ruan, Youyi Zheng, and Hui Huang. Sketchformer++: A hierarchical transformer architecture for vector sketch representation. In *International Conference on Computational Visual Media*, pages 24–41. Springer, 2024. 2
- [37] Lumin Yang, Jiajie Zhuang, Hongbo Fu, Xiangzhi Wei, Kun Zhou, and Youyi Zheng. Sketchgnn: Semantic sketch segmentation with graph neural networks. *ACM Transactions on Graphics (TOG)*, 40(3):1–13, 2021. 5
- [38] Rui Yang, Xiaojun Wu, and Shengfeng He. Mixsa: Training-free reference-based sketch extraction via mixture-of-self-attention. *IEEE Transactions on Visualization and Computer Graphics*, 2024. 2
- [39] Kwan Yun, Youngseo Kim, Kwanggyoon Seo, Chang Wook Seo, and Junyong Noh. Representative feature extraction during diffusion process for sketch extraction with one example. *arXiv preprint arXiv:2401.04362*, 2024. 2
- [40] Kwan Yun, Kwanggyoon Seo, Chang Wook Seo, Soyeon Yoon, Seongcheol Kim, Soohyun Ji, Amirsaman Ashtari, and Junyong Noh. Stylized face sketch extraction via generative prior with limited data. In *Computer Graphics Forum*, page e15045. Wiley Online Library, 2024. 2
- [41] Sicong Zang, Shikui Tu, and Lei Xu. Self-organizing a latent hierarchy of sketch patterns for controllable sketch synthesis. *IEEE Transactions on Neural Networks and Learning Systems*, 2023. 2
- [42] Biao Zhang, Jiapeng Tang, Matthias Niessner, and Peter Wonka. 3dshape2vecset: A 3d shape representation for neural fields and generative diffusion models. *ACM Transactions On Graphics (TOG)*, 42(4):1–16, 2023. 2, 3
- [43] Longwen Zhang, Ziyu Wang, Qixuan Zhang, Qiwei Qiu, Anqi Pang, Haoran Jiang, Wei Yang, Lan Xu, and Jingyi Yu. Clay: A controllable large-scale generative model for creating high-quality 3d assets. *ACM Transactions on Graphics (TOG)*, 43(4):1–20, 2024. 3
- [44] Richard Zhang, Phillip Isola, Alexei A Efros, Eli Shechtman, and Oliver Wang. The unreasonable effectiveness of deep features as a perceptual metric. In *Proceedings of the IEEE conference on computer vision and pattern recognition*, pages 586–595, 2018. 4

# StrokeFusion: Vector Sketch Generation via Joint Stroke-UDF Encoding and Latent Sequence Diffusion

## Supplementary Material

### A. Stroke-Conditioned Sketch Generation

Figure 9 showcases conditional generation results from categories including airplane, umbrella, face, pizza, apple, and moon. We fix the stroke with the highest number of path points in the dataset as a condition and generate the remaining parts by replacing the denoised version with the noised ground truth during the diffusion process. While the quality of these completions is lower compared to fully unconditional generation (due to inherent task difficulty and potential conflicts between fixed and generated strokes), the results demonstrate our model’s ability to semantically understand and coherently extend stroke-based structures.

### B. Additional Randomly Generated Results

Figure 10 presents qualitative visualization results for all training categories, covering a range of stroke complexities: low-stroke (*apple, moon, shoe, umbrella, fish*), medium-stroke (*chair, airplane, television, face, bus*), and high-stroke (*pizza, spider, cat, train*). Our method effectively generates recognizable contours with intricate details. For high-stroke objects, the model successfully coordinates the positional and directional relationships among multiple strokes, as exemplified by pizza slice lines and spider legs.

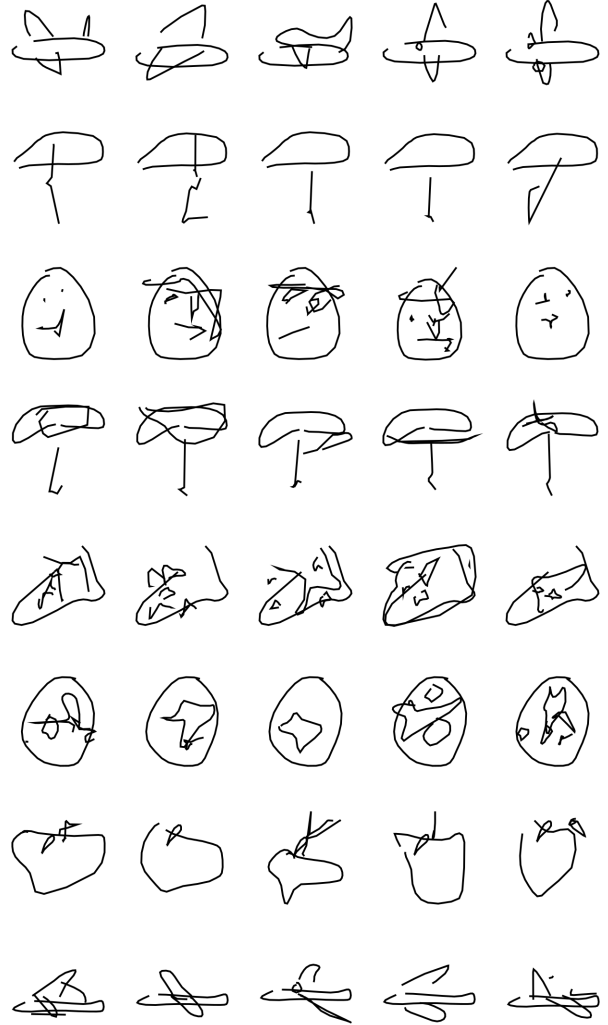


Figure 9. Examples of Stroke-Conditioned Generation

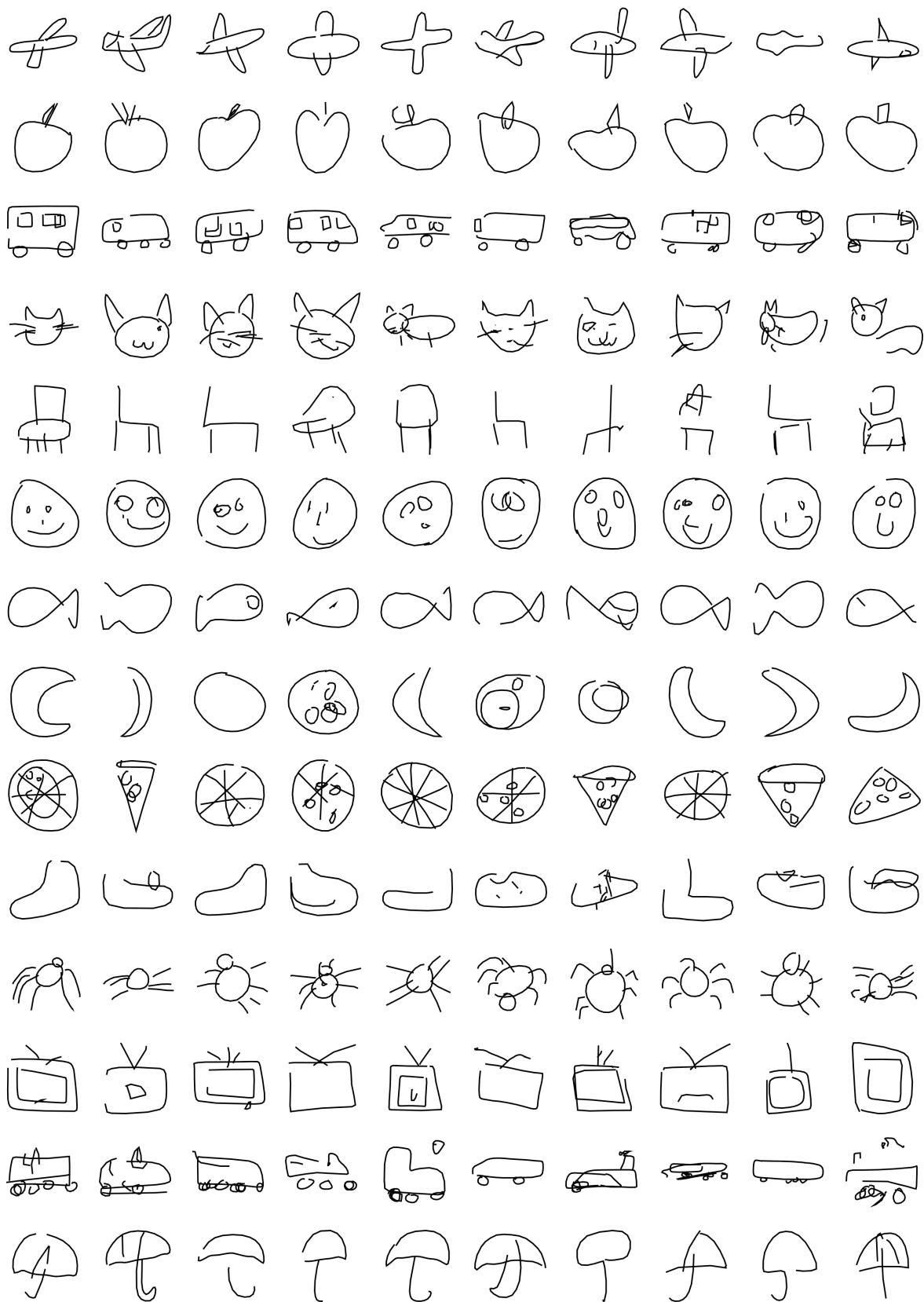


Figure 10. Additional randomly generated sketch results using our method.